Applied Ocean Research 102 (2020) 102248

Contents lists available at ScienceDirect

Applied Ocean Research

journal homepage: www.elsevier.com/locate/apor

Computer vision and thermal monitoring of HMPE fibre rope condition during CBOS testing

Shaun Falconer*[,a], Ellen Nordgård-Hansen[b], Geir Grasmo[a]

[a] Department of Engineering Sciences, University of Agder, Grimstad NO 4876, Norway
[b] NORCE Norwegian Research Centre AS, Grimstad NO 4876, Norway

ARTICLE INFO

Keywords:
HMPE Rope
Condition monitoring
Computer vision
Thermal imaging
CBOS
Offshore lifting

ABSTRACT

Fibre rope usage in deep sea lifting operations is gaining more prominence in recent times. With rope minimum break loads (MBL) comparable to that of their steel wire counterparts, the use of high modulus polyethylene (HMPE) ropes is seen as a viable option for use in subsea construction cranes. The ropes are worn out during use and visual inspection remains one of the main methods of determining whether a fibre rope is to be retired from use, therefore a natural extension is condition monitoring through computer vision. Creep and temperature are constraining with HMPE ropes and should be monitored continuously, particularly when the rope is cyclically bent over sheaves. Additionally, interpreting the thermal history of the rope during use could give insight into deterioration. In this paper, a condition monitoring system based on combined computer vision and thermal monitoring is used during cyclic bend over sheave tests performed on 560 kN break load of 12 strand braided HMPE ropes. New monitoring features such as local length and width through computer vision algorithms combined with surface thermal monitoring and global elongation are presented and their effectiveness as condition monitoring features is assessed.

1. Introduction

Fibre ropes are increasingly gaining recognition as a viable alternative to steel ropes for use in deep sea lifting operations. High Modulus Polyethylene (HMPE) ropes have been shown to have about the same mechanical properties as those of steel ropes, but with other potential benefits and constraints. Due to its lighter weight and almost neutral buoyancy, HMPE ropes can be used in subsea construction cranes to exceed the depth limits imposed by steel rope sage. Additionally with their greater ease of handling and lighter weight, there is potential to use smaller cranes and vessels in lifting and subsea deployment operations.

The first issue with HMPE from an endurance perspective is failure by creep. The three main parameters that effect creep in HMPE ropes are a combination of the load, temperature and time of usage. Depending on the size of payload, type of lifting operation and environment where the lift takes place, the extent at which creep influences deformation behaviour in ropes can vary greatly. HMPE rope typically has a maximum working temperature of 65 °C, on which exceeding this limit will lead to deterioration of the material through temperature alone.

The second issue is failure through wear. Offshore lifting operations involve periods where active heave compensation occurs when deploying a payload subsea. The rope will be subject to cyclic bend over sheaves (CBOS), where it is continually driven back and forth over sheaves, the severity of which will be influenced by load size and sea state. In addition to heat generation from bending deformation, friction from both inter-strand motion and sheave contact will contribute to heat generation during operation. Due to the plethora of potential damage mechanisms that have potential to influence the remaining useful life (RUL) of the rope, condition monitoring for this regime requires particular attention through a combination of methods.

Fibre rope for usage in maritime operations is not a novel concept but their application to deep sea lifting operations is a fairly recent development. Applications in vessel and offshore structure mooring are detailed in current standards set by industry, however their application in lifting operations and associated discard criteria is mentioned briefly. DNV-RP-E304 [1] details how the damage of the fibre rope must be assessed, where each constituent substructure (i.e filament, strand, subrope, etc) has to be checked by manual inspection and then re-classified or discarded based on inspector judgement. CI 2001-04 [2] provides a thorough guide of fibre rope damage types and mechanisms for inspectors. DNVGL-OS-E303 [3] states that if a rope has been subjected to 70% of its minimum break load (MBL), then the rope has to be retired

* Corresponding author.
E-mail address: shaun.falconer@uia.no (S. Falconer).

https://doi.org/10.1016/j.apor.2020.102248
Received 12 August 2019; Received in revised form 5 June 2020; Accepted 5 June 2020
Available online 07 August 2020

or re-certified. DNV-GL-ST-E407 [4] requires that fibre rope used in deployment and recovery systems must have all its physical properties detailed, including potential failure modes, to be certified. Finally, the 3-T parameter developed by DNV-GL [5] is used to obtain a linear relationship between tension and time-to-rupture by evaluating the logarithmic time-to-rupture as a function of tension at a given temperature. However to investigate if longer RUL for deepsea lifting fibre rope is possible, a continuous means of monitoring with thorough data interpretation must be developed, rather than a simple re-classification or re-certification.

Extensive CBOS testing is beneficial to explore RUL. Davies et al [6] presented the results of testing on HMPE braided rope of 19 mm nominal diameter from which an empirical model for RUL was derived, though it is acknowledged that further testing is required on ropes of larger diameters to qualify their method for lifting operations.

Given that visual inspection is common for fibre rope, use of computer vision can potentially replace manual inspection. Hearle et al [7] used a webcam to monitor the strains in yarns during testing. Since machine vision technology has improved after their work, there were obvious limitations in the equipment used, but they showed the possible application of computer vision and image processing for fibre rope monitoring. Additionally, Ghoreishi et al [8] used computer vision and image processing as one of their three independent measuring systems for extensometry during tension-torsion testing to validate their analytical model of rope behaviour. For steel wire ropes, Söhnchen [9] details a system for visual inspection of ropeways and mining shafts from four different perspectives to analyse lay length, diameter, and wire breaks. Yaman and Karakose [10] proposed image processing for monitoring steel rope in elevator systems, where fault detection was performed by analysing the auto-correlation signals of pixels in the rope images to detect wire breaks.

Assessment of rope geometric parameters has been used in other fibre rope monitoring systems. For example, Mupende and Zerza [11] made a patent where the diameter of the rope for lifting operations is monitored using clamping roller set up and position sensor with a warning activated at a user-defined discard criteria, along with length change estimations. Van der Woude and Zijlmans [12] proposed as monitoring system for offshore lifting operations (using steel rope as an example), where the device can take cross-sectional area measurements and log its position along the rope. Ernst et al [13] also detail embedded methods for monitoring of elongation of discrete sections of fibre rope where bending occurs in operation and replacing the rope subject to exceeding a pre-set limit.

Additionally, it is important to distinguish between the sections being monitored via some form of marking system throughout the length of the rope and monitor them for changes. De Angelis [14] proposes a system to replace fibre rope based on the deterioration of markers and evaluate them by visual inspection. In addition to this, Logan et al [15] detailed a patent for having markers on load bearing members for elevators such as rope, with the spaces between these markers being monitored for strain and fatigue.

Temperature measurement of fibre rope for lifting operations is of paramount importance due to material limitations in maximum temperature. Active heave compensation in offshore construction cranes will cause heat generation in the rope if a payload is held at the same depth subsea for extended periods of time. In terms of thermal monitoring of fibre rope, Törnqvist et al [16] analysed rope samples during CBOS testing with embedded thermocouples and an IR camera. However, both are mainly used to observe the effects of water cooling on the rope samples, in order to ensure that they do not reach critical temperature. In addition to this, Davies et al [17] include some results from IR camera during CBOS testing to try to couple rope properties and temperature changes, however references are only made regarding the change in temperature in ropes during dry and wet tests. Additionally, Nordgård-Hansen et al [18] explored the use of chemometrics as method for quantifying aging in fibre ropes based on infrared images recorded using some of the ropes tested as part of the campaigns outlined in this paper, including providing extensive review of possible explanations for observed changes as the rope deteriorates. De Angelis [19] proposed using a conductive thermal element and provides a warning to the user if a critical temperature is exceeded. More recently, Ning et al [20] used embedded thermocouples inside and outside of several different rope samples during CBOS testing by evaluating thermal damage through varying test conditions and its subsequent influence.

Manual inspection of rope without thorough knowledge of its use history has significant potential for waste through premature retirement. Deterioration in fibre ropes through CBOS deformations results in length, width and temperature changes that require monitoring throughout use. This paper builds upon previous work [21] performed at the University of Agder, where computer vision techniques were used to monitor rope width and length in tension-tension tests.

Improved monitoring systems are the first steps in developing more informed RUL estimations and subsequently avoiding fibre rope waste. Still, there is currently no single detailed study of a combined computer vision and thermal monitoring method for fibre ropes under a CBOS regime. In the present work, data is extracted through image processing algorithms to monitor changes in local length and width for fibre ropes. It has been confirmed that there is local motion of strands during usage, and the methods applied allow the continuous monitoring of this movement. The geometric data is combined with temperature measurements, which show corresponding changes over time. This work may therefore serve as the basis for a potential monitoring system to be implemented in an offshore crane.

Test details are given in Section 2, and the algorithms from previous work have been modified, as presented in Section 3. These algorithms are then applied to data recorded during CBOS testing. The results of local length, width and temperature monitoring in different bending zones in five ropes during CBOS testing are presented in Section 4, and their effectiveness with regards to rope condition is discussed in Section 5, before further work is considered and conclusions offered.

2. Monitoring methods and materials

The condition monitoring set-up and feature selection were evaluated on ropes during CBOS testing. The test machine used was installed by DEP Engineering at the Mechatronics Innovation Lab (MIL) in Grimstad, Norway, see Fig. 1. The machine is capable of testing both steel and fibre ropes between 20 and 30 mm diameters and can deliver a maximum line pull of 150 kN. The tension is kept constant by a hydraulic cylinder that extends as the test progresses to compensate for creep. The test and driving sheaves have diameters of 0.8 m and 1.0 m respectively. The test sheave is made from 42CrNiMo4 steel and has a U-profile.

The condition monitoring set-up consists of three parts. A computer vision system with four cameras asymmetrically positioned around the rope, was used to record videos of the rope next to the test sheave end approximately every 1000 cycles. Each camera recorded 2000 images in each video recording, which corresponds to 13–15 complete cycles. As seen in Fig. 2, the rope is not centered in the camera frame, due to the testing sheave being slightly angled.

A FLIR A6753sc infrared thermal camera recorded rope surface temperature periodically as the tests progressed. It was placed approximately 50 cm from the rope entrance to the sheave profile. The recording process was set to sample at 100 Hz for 2000 images, resulting in a 20 seconds video for each period. This was sufficient to record at least one full cycle in the CBOS test. The data was then interpreted using FLIR ResearchIR Max 4 software and then converted to CSV format.

Finally, an infra-red distance sensor monitored the increase in length of the CBOS machine hydraulic load cylinder over the duration of the test.

Fig. 1. CBOS test machine as located the MIL, Norway. View is from just behind the test sheave with the driving sheave visible at the far end of the test frame.

Further details regarding the specification of the optical cameras, thermal camera and distance measuring laser are available in Table 3, Table 4 and Table 5 respectively in Appendix A.

The section of the rope that never reaches the sheave, thus never bends, is called the straight zone (SZ), while the rope section that touches the sheave and bends only once before the sheave changes direction is called the single bend zone (SBZ). Finally, the rope section that bends across the sheave and is straightened again below the sheave before the sheave turns, is called the double bend zone (DBZ). Colour coded markers were sewn into each of these zones, see Fig. 3. These markers were used to monitor the changes in local length at these positions, in addition to the widths. The thermal measurements were also taken from these zones.

The procedure was to guide the rope over both the driving and test sheave with the ends attached to opposite sides of the trolley that moves along the test bench between the sheaves. The spliced eye loops were placed over 56 mm diameter steel pins in the connector attached to the trolley to hold the rope in place. Care was taken to ensure there was minimal twist in the rope. The first 1500 cycles were used to bed in and as a ”calibration” phase for the camera set-up, in which camera parameters where adjusted for lighting conditions and to ensure that good quality data was recorded automatically. After this phase, the test was run until failure. A failure was considered to occur when there was a substantial loss of tension on the cylinder, causing the test to stop automatically or when there was a more obvious rupture.

The ropes used were 12 strand Dyneema®DM20 XBO HMPE fibre ropes with nominal diameter of 28 mm and the minimum break load

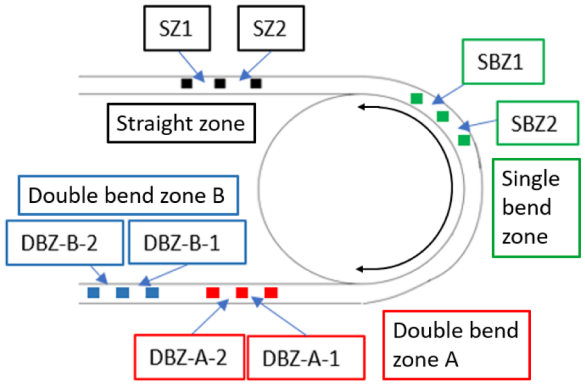

Fig. 3. The approximate location of the colour-coded markers placed on the rope for localised length and width monitoring.

(MBL) was 560 kN. They were approximately 22.2 m long, spliced at each end over a 2.2 m length with eye loops, and tested on a constant 50 kN line pull over approximately 4.2 m stroke length.

3. Theory and data interpretation

3.1. Computer vision system and image processing

The algorithms used for image processing and data analysis were developed in Python using the OpenCV library [22]. The data is interpreted from videos recorded during each CBOS test. During a post-processing phase, a series of morphological operations were performed to calculate the local length and width of the rope.

3.1.1. Local length of rope sections

The local length of each subsection is calculated by locating the different coloured markers sewn into the rope. The image is converted to HSV colour scaling for ease of detecting colours at varying levels of brightness. A specific colour is selected using this colour regime (”red” in the case of the operations shown in Fig. 4). This scale is modified in the algorithm to detect the other colours coinciding with the other zones of interest on the rope. A binary image is created, where the sections of the image that coincide with the colour mask are converted to white. A dilation operation is performed to fill in the gaps in the colour mask and the marker centre points are found using a contouring operation. The Euclidean distance between centre points of both markers is then calculated. The operations are summarised in Fig. 4.

It is attempted to find at least ten images of each subsection in each video recording. The median, maximum, minimum and variation as standard deviation of the length across these images is calculated and are used as the values to represent the strain of the rope at that specific time stamp. These distances are monitored for changes as the test proceeded.

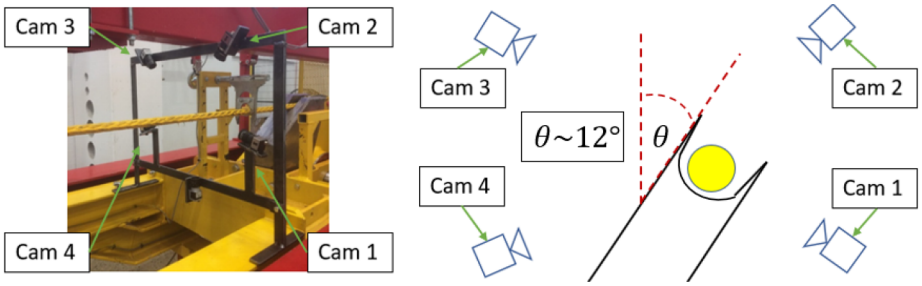

Fig. 2. The computer vision set up with the four cameras used positioned around the rope. The accompanying schematic shows the designated camera labels for each position and roughly how they are positioned with respect to the rope and sheave access.

Fig. 4. Different stages and effects of morphological operations applied to the image to detect a specific colour for length measurements: (a) original image, (b) binary image created, (c) dilation operation applied and (d) final processed image with centre point of marker visible after contouring operation.

3.1.2. Rope widths

Rope cross section width was calculated from the perspective of all four cameras. The width calculation works in a similar fashion to the length algorithm, except it is the rope colour that is detected in the processing stage. The widths along the whole length of rope visible in the computer vision system are calculated at the SZ, SBZ and DBZ sections.

As with the local length calculation process, the image is converted to HSV representation, however the colour of the rope is searched to distinguish it from the background and the different coloured markers. The image is then dilated to fill in any gaps that may be present and eroded to better coincide with the edges of the rope. Finally, the edges of the rope are detected using a contouring operation which is then applied to the original image. Images of selected operations are shown in Fig. 5.

The curves that are detected in the vicinity of the rope edges are saved as coordinates. Seven regions of interest are defined for each image, and within these specific areas the shortest distance from the top line to the bottom line to be saved as the view width. The median of the resulting seven values is defined as the width measurement of this section length. The maximum, minimum and standard deviation of these seven measurements are also measured. Fig. 6 shows an example of this fully processed image with complete widths found in each specific region of interest.

The cameras are synchronised, therefore allowing the widths from all four perspectives to be directly compared at the same time and point along the rope.

3.1.3. Unit conversion

The cameras are asymmetrically placed around the rope at different distances. Since Python OpenCV's default measurement is in pixels, the cameras readings have to be scaled. The estimation for this conversion is made by placing a metre reference next to the rope at the beginning of each test.

3.2. Thermal imaging of rope surface

Fig. 7 shows an example of a screen shot from the FLIR software. In this particular example the rope has already been subject to CBOS motion and the various levels of temperature are shown, with the light and dark sections representing the higher and lower temperatures respectively. A region of interest (ROI) is defined, where the average temperature is determined from the pixels located within it. This particular region is chosen so it will always contain only rope and no background during the slight varying vertical displacements of the rope.

3.2.1. Outliers

Outliers in the geometric features are handled through using the median absolute deviation (MAD) as shown in Eq. 1. This is applied to the local length and width data due to these measurements comprising of readings from several images of the same sections at each time stamp.

$$\mathrm{MAD} = \mathrm{median}(|x - \tilde{x}|) \tag{1}$$

Where x is each value and $\tilde{x}$ is the median value of the recorded data set.

This approach is chosen since it is more robust to outliers than using the average of the measurements. It is possible to eliminate these outliers from the data set based on a defined limit shown in Eqn 2:

$$|x - \tilde{x}| \geq 3 \times \mathrm{MAD} \tag{2}$$

The median, maximum, minimum and standard deviation of the values that remain after the application of MAD are used as the feature values at each particular time stamp.

Outliers in the thermal data are limited by the conservative ROI applied during recording. The data collected is limited to the rope surface area with no interference from the background in the images.

3.2.2. Missing data

Once outliers are omitted, the data set is treated for missing data. Missing data may occur as a result of instrumentation failures or the algorithms failing to detect the specific sections of the rope due to degradation of section markers.

Imputation via linear interpolation is implemented, replacing the missing data through interpolation in each respective feature over the whole test time of each individual rope. A rolling mean of 3 steps is applied before presenting the local length and width results to maintain the general trend of the measurements throughout the monitoring period.

3.2.3. Summary of recorded data

Table 1 gives a summary of the data are recorded for each step by the condition monitoring system.

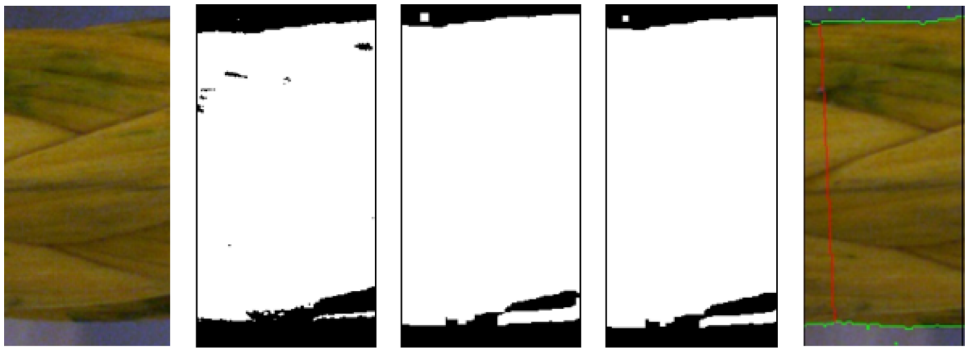

Fig. 5. Different stages and effects of morphological operations applied to the image to detect the rope and calculate the width: (a) original image, (b) binary image created, (c) dilation operation applied, (d) erosion to reduce edge thickness, (e) contouring to find edges of rope and applied to original image to find the width (red line). (For interpretation of the references to colour in this figure legend, the reader is referred to the web version of this article.)

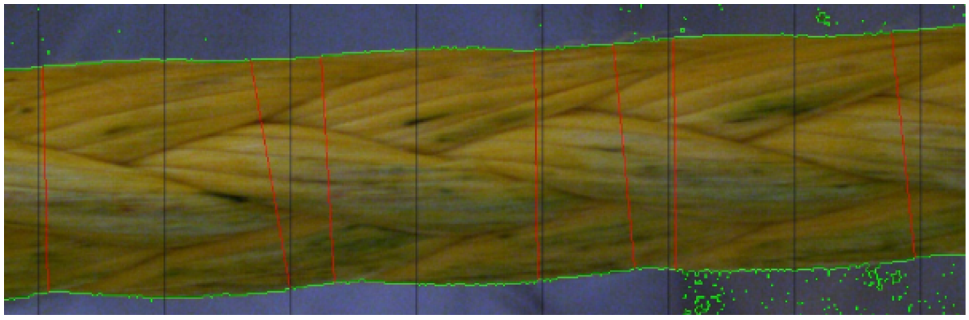

Fig. 6. Example of a processed image with the seven regions of interest applied and widths detected.

4. Results

4.1. Initial observations

Table 2 shows the number of cycles each rope sample reached before failure in the CBOS machine tests. These numbers are thus the number of cycles to failure (CTF). All the ropes are the same type. (Rope no. 1 and no. 2 were used for different process and test developments and results are thus excluded.)

Fig. 8 shows images of the typical state of the rope after each testing phase and removal from the CBOS machine. The top image is an example of the surface compression damage done to the rope through contact with the sheave. The bottom image is the other side of the rope that did not get in contact with the sheave. From this view, the ruptured strands and extruded loops are visible. These become more apparent as the rope degrades during the test.

Fig. 9 shows the global elongation for the ropes tested. The extension of the rope is based on the changes in length of the hydraulic cylinder keeping tension on the rope as measured by the IR laser. This extension is then interpreted as general rope elongation using the ropes' original length as starting point.

It is noted that Ropes 3 and 6 failed due to degradation in the splice that was partly running over the larger driving sheave. The other ropes all failed at the test sheave as intended. Note that the global elongation in all cases is below 1%, which is in accordance with the manufacturer's rope specification.

4.2. Computer vision system and image processing

4.2.1. Local length

Figs. 10 and 11 show the results of the relative local nominal length for Ropes 3 to 7, in sections DBZ-A and DBZ-B respectively. In each figure, the elongation changes (local strains) as detected by the algorithm for each rope are shown and compared. These are shown against the time, starting from just after the initial bedding in phase until just before failure occurred in the rope specimen. The % local length measurements are based on the changes from the original length of each respective subsection from the end of the bedding in phase. The changes for the SZ and SBZ sections are not presented as they were negligible in comparison to the DBZ-A and DBZ-B sections.

From Figs. 10 and 11 it is seen that local distances between the markers vary and increase over time. Overall the strands are shown to heterogeneously displaced in the DBZ sections. However in Ropes 4, 5 and 7 there are reciprocal changes in the DBZ, where a decrease in one subsection is accompanied by an increase in adjacent subsection. Rope 7 in particular shows the largest changes in local distance compared to the other rope samples.

Table 1
Data recorded by condition monitoring system.

Length	Width 1	Width 2	Width 3	Width 4	Temperature
SZ-1	SZ-1	SZ-1	SZ-1	SZ-1	SZ
SZ-2	SZ-2	SZ-2	SZ-2	SZ-2	SBZ
SBZ-1	SBZ-1	SBZ-1	SBZ-1	SBZ-1	DBZ
SBZ-2	SBZ-2	SBZ-2	SBZ-2	SBZ-2	
DBZ-A-1	DBZ-A-1	DBZ-A-1	DBZ-A-1	DBZ-A-1	
DBZ-A-2	DBZ-A-2	DBZ-A-2	DBZ-A-2	DBZ-A-2	
DBZ-B-1	DBZ-B-1	DBZ-B-1	DBZ-B-1	DBZ-B-1	
DBZ-B-2	DBZ-B-2	DBZ-B-2	DBZ-B-2	DBZ-B-2	

Table 2
Number of cycles to failure (CTF).

Rope no.	3	4	5	6	7
CTF	75 324	122 368	120 430	87 314	143 374

4.2.2. Width

The % change in relative width measurements are based on the changes from the original width of each respective subsection. Fig. 12 shows the relative change in width at DBZ-A-1 subsection across all five ropes against time from after the initial bedding in phase until rupture. It also shows that the smallest total relative width changes, when comparing initial and just-before-rupture values, occurred in Ropes 3 and 6, which ran for shortest duration. Substantial varying measurements compared to the other ropes were also observed for this subsection in Rope 4. Camera 2 coincides with viewing from above the rope directly along the sheave axis. Views from the other cameras showed the same tendency of increased width as a function of time, but to a lesser degree.

Examples of relative width change from camera 2 across all sections with respect to time are shown in Figs. 13 and 14 for Ropes 5 and 7 respectively. The other ropes showed a similar separation between SZ and SBZ showing minor changes, and DBZ sections showing increasing width measurements with the progression of testing. In the SZ section in both examples there is slightly reduced width due to rope elongation.

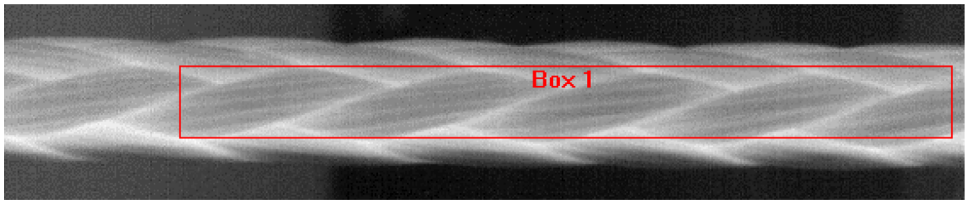

Fig. 7. Screen shot from FLIR ResearchIR Max 4 software with the ROI defined for average temperature calculation.

Fig. 8. Compression damage (top) and extruded loops (bottom).

This similarly occurs in the SBZ section in both examples, however there are increases in the width detected in some subsections towards the end of the monitoring period.

In general, width changes in the SZ and SBZ sections do not exceed 5%, whereas the DBZ section width changes are shown to have reached 10% and more.

4.3. Thermal imaging

Figs. 15 to 16 show the results for the average, maximum, minimum and standard deviation of the temperatures measured in the ROI defined in Fig. 7 for Ropes 4 and 7 respectively at different times during testing.

Each curve represents the temperature measurements of the rope sections visible to the thermal camera as it is cycled back and forth over the sheave. The measurement starts in the SZ section, with the mid point in the DBZ section, then cycles back to the SZ section.

In Rope 4, the average temperature in both the SBZ and DBZ sections measured at 289 hours has decreased in comparison to the temperatures at 162 and 192 hours. Additionally, the DBZ section is shown to have a lower maximum temperature and minimum temperature compared to the measurements at 162 and 192 hours.

Similarly in Rope 7, the average, maximum and minimum temperatures in the DBZ section measured at 338 hours are lower in comparison to the measurements at 34 and 167 hours. The SBZ average, maximum and minimum temperatures at 34 and 338 hours are observed to be similar values. This behaviour is discussed later.

5. Discussion

In order to monitor the rope state, CBOS testing is used as it can represent rope use during offshore lifting operations. Focus is put on evaluating adequate monitoring methods that can potentially be applied for field use.

5.1. Local length

5.1.1. Findings

For all five ropes tested the sections monitored in the straight zone (SZ) and single bend zone (SBZ), there were no strains that exceeded 1% of the original length. Ropes 4, 5 and 7 ran for significantly more cycles than Ropes 3 and 6, with significant longer elongation detected in the two DBZ sections than the SZ and SBZ sections. This can be attributed to DBZ sections being subjected to twice as many bends over the sheave than SBZ.

Figs. 10 and 11 show the changes detected using the length calculation method throughout each test, with Rope 7 displaying the largest changes in the marked DBZ sections. There is observed to be a heterogeneous spread of strain changes in the DBZ sections across all the samples, most severe for DBZ-A in Rope 7.

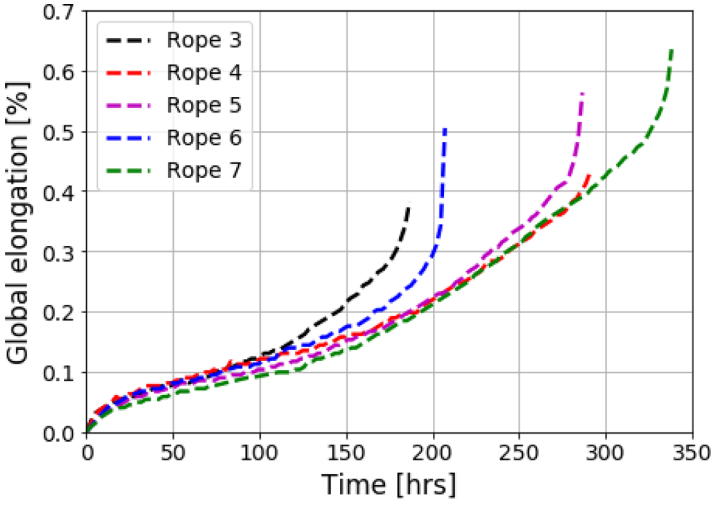

Fig. 9. Global elongation of the ropes after bedding in.

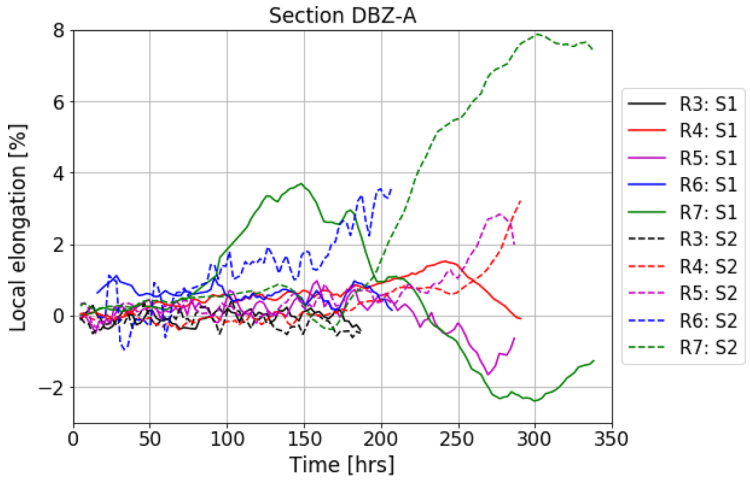

Fig. 10. Local length changes after bedding in phase in Section DBZ-A for all ropes (R-Rope, S-Subsection).

Local length changes are attributed to rope structure rearrangement as the test progresses as well as to actual fibre creep. Extruded loops occur as strands are bunched together with the flexing-unflexing movement during bending, pulling portions of the sub-rope through the whole structure, resulting in length changes at the local scale. The strands also rupture and fuse, contributing to rearrangement of the rope morphology.

Figs. 17 and 18 are examples taken from the processed data and show the significant changes in both length and rope structure from the first to the final length measurements. There are instances of "reciprocal" changes where one subsection increases or decreases in length and the corresponding opposite behaviour occurs in the continual subsection. The subsections show strands move between each other and give rise to heterogeneous displacement of markers.

5.1.2. Uncertainties and error sources

The markers used for detection are not guaranteed to be placed at the exact same position relative to the test sheave on each rope, contributing to variations in the measurement results.

The deterioration of the rope condition causes displacement in the position of the rope with respect to the camera position, for example in Rope 5 where there was pronounced twist before failure. Such displacements of the rope will contribute to variation in the local length and width measurements.

The algorithm relies on finding the centre point of each marker. The wear on these markers while testing progresses can have an effect on the lengths measured. It is acknowledged than any reduction in size of these markers is insignificant compared to the change in length of the subsection. The number of tests conducted are too few to quantify the errors so far.

5.1.3. Application to condition monitoring

The heterogeneous local length changes observed between ropes, across the DBZ sections in particular, indicate that rope condition monitoring must be addressed at strand level. What the rope experiences during CBOS motion defines what the system must be capable of monitoring. The present method is shown to be able to reliably track the changes in local length during testing, allowing local length to be properly mapped during rope lifetime.

The majority of local length changes over 1% came after half the rope lifetime, thus this could serve as warning and call for further inspection when the total subsection length exceeds this value, as well as an aid to subsequent decision making.

In Figs. 17 and 18, local relative distortion of the strand is shown to be -11.4% and +10.8% in the DBZ-B-1 and DBZ-B-2 subsections respectively when comparing the first and final measurements. The overall middle relative distortion equates to -0.6% across the whole lay length in DBZ-B, highlighting the need for sub-lay length

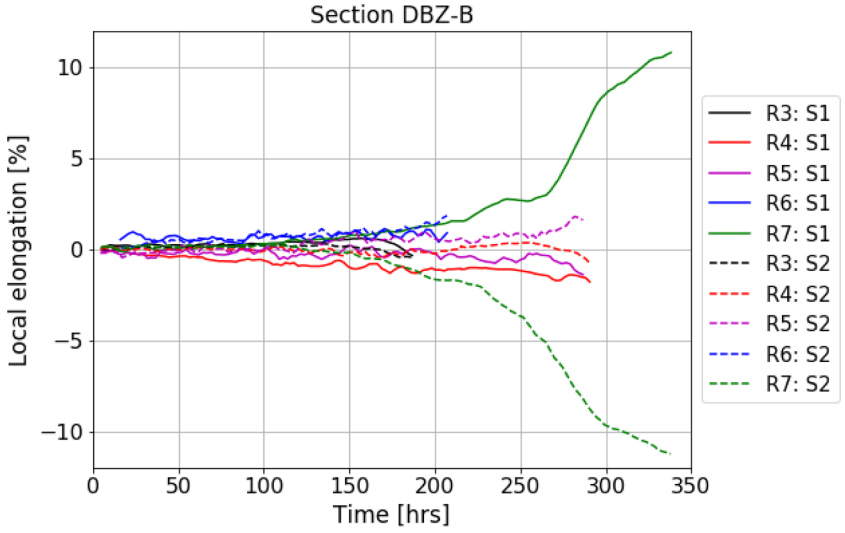

Fig. 11. Local length changes after bedding in phase in Section DBZ-B for all ropes (R-Rope, S-Subsection).

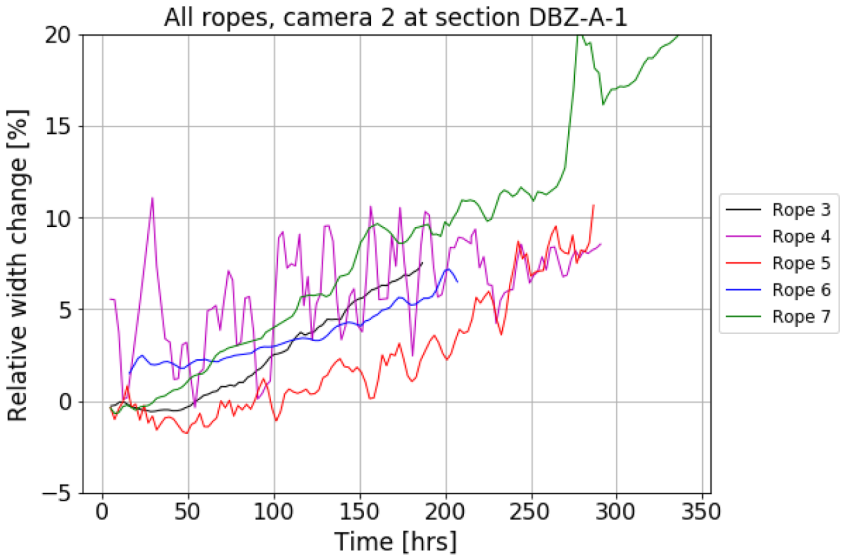

Fig. 12. Percentage change in width from camera 2, perpendicular to sheave axis, at position DBZ-A-1 for all ropes.

measurements.

The presented method is effective at monitoring the local length changes and also provides a useful visual aid to rope deterioration and how the related subsections interact with each other at strand level.

5.2. Width

5.2.1. Findings

Extruded loops and ruptured strands become more apparent in the DBZ sections due to repeated bending and unbending, which are detected effectively by the visual system and algorithm through the larger relative width change. The structure of the rope rearranges due to repeated deformation. It is noted that generally there are small variations and continuous increase in width despite the elongation of the same sections.

Unlike the local length measurements, there is no evidence of ”reciprocal” changes. Each subsection is shown to follow the trend of the neighbouring subsection despite the occurrence of the opposite elongation behaviour in some of the ropes.

After inspection of the processed images from Rope 4, there is visible evidence of substantial twist in the rope, explaining the observation of varying widths for Rope 4 in section DBZ-A-1.

5.2.2. Uncertainties and error sources

The rope will not maintain the exact same perspective to the camera due to slight rotation while testing. Since several hours pass between each recording, it is possible that the portion of the rope in contact with the sheave changes.

The rope colour also changed slightly during degradation, meaning that edge detection created from applied binary image created through the colour mask may not resemble the ”true” edge of the rope.

Imputation is used to compensate for missing data and can add uncertainty as it is just an interpolation. However the rolling mean smoothing process helps to show the ”general trend” in width change with these values included.

5.2.3. Application to condition monitoring

Width monitoring is vital as it indicates changes in rope structure, including both in shape or through deterioration such as extruded loops or ruptured strands. The width calculation method applied is adept at monitoring these changes over the testing period, and it also clearly displays the differences in the different bending zones.

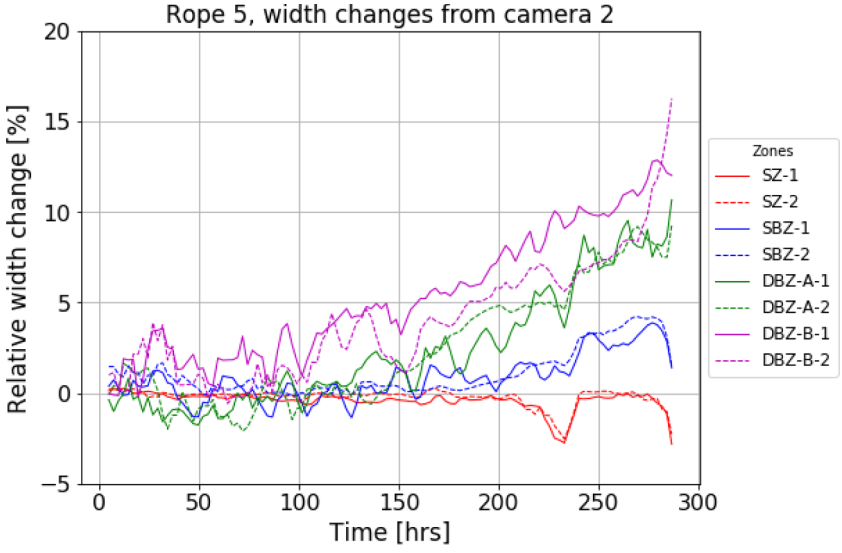

Fig. 13. Percentage change in width from camera 2 for all zones in Rope 5.

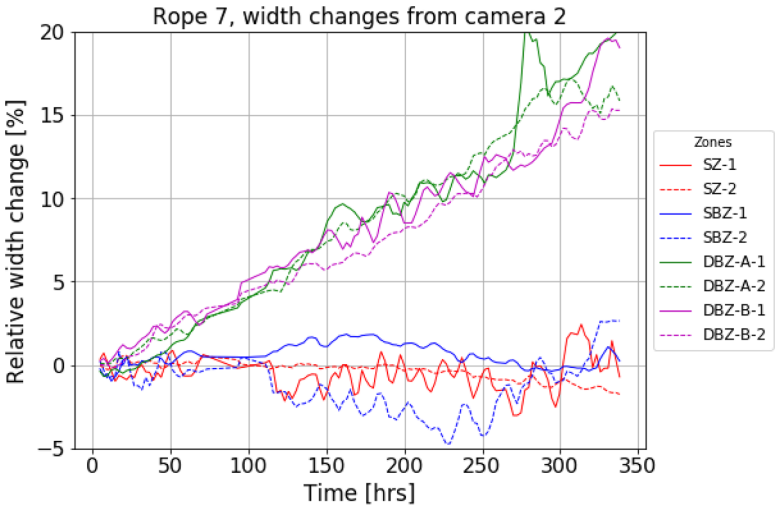

Fig. 14. Percentage change in width from camera 2 for all zones in Rope 7.

An example of a processed image is shown in Fig. 19 from Rope 3 as observed from Camera 3. There is visible deterioration in the rope structure with the presence of extruded loops clearly seen before rupture. The width calculation algorithm adapts to this, with the rope edge detection including the extruded loops. In this instance, the shortest distance in the constituent regions of interest will be higher and subsequently produce a larger median value, allowing the changes to be quantified throughout the rope lifetime.

Substantial movement of the rope could be a sign that significant deterioration or structural rearrangement has occurred during use. Monitoring these variations using this method can find use as an aid to decision making regarding discard or re-classification of the rope in use, as well as documenting the exact location of damage accumulation along the rope. Using the applied method it is straight-forward to gauge trends in width change and inspect the images that coincide with the measurements.

5.3. Thermal imaging

5.3.1. Findings

Thermal images are recorded as they indicate frictional and deformation work in the rope. Figs. 15 to 16 show a distinct temperature measurement curve in each rope. However, within each recording there are distinct zones visible due to temperatures associated with the bending behaviour in each section. The first and second plateaus in the curves are associated with the SBZ and DBZ sections respectively.

After increasing from the beginning of the test, the average temperature in the DBZ section is shown to decrease as the rope heads toward rupture. This also coincides with lower maximum and minimum temperature at the DBZ section at the more advanced recording times during testing.

The varying temperatures in the sampling areas of the rope surface are given by the standard deviation. This follows the same ”plateau” pattern as the temperatures. There are larger deviations recorded in the DBZ sections at the more advanced recording times in Ropes 4 and 7. However, the deviations are approximately the same in the SZ section for the recording times in Rope 4 but are larger in Rope 7. Additionally in the transfer points between the SZ and DBZ sections in Rope 7 show larger variations.

5.3.2. Uncertainties and error sources

The thermal camera is placed at approximately the same distance from the sheave entrance for each test but slight variations in distance from the rope are possible. The camera distance from the rope is measured for each rope, and input to the camera software, so these movements do not influence the accuracy of the recorded temperatures.

Similar to the local length and width measurements, differences in the rope mounting can also lead to slight variation in values recorded.

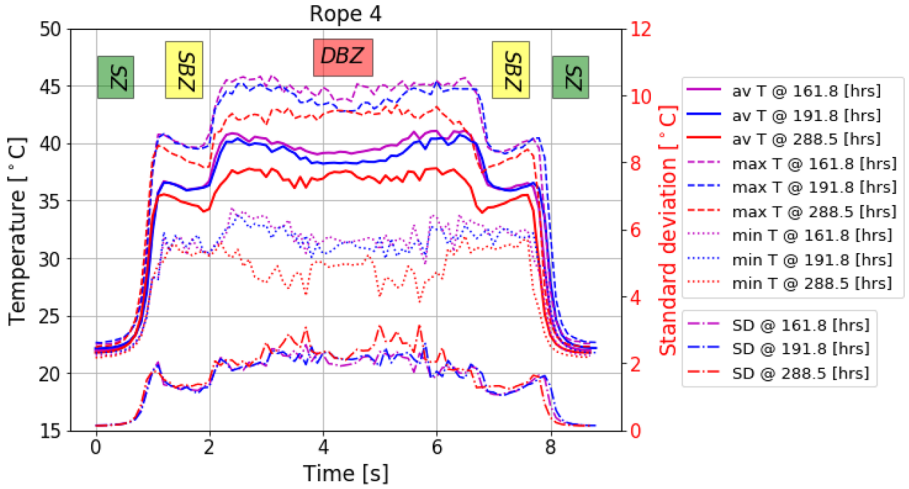

Fig. 15. Rope 4 average, maximum, minimum and standard deviation temperature measurements along the rope for one cycle with respect to the associated test time.

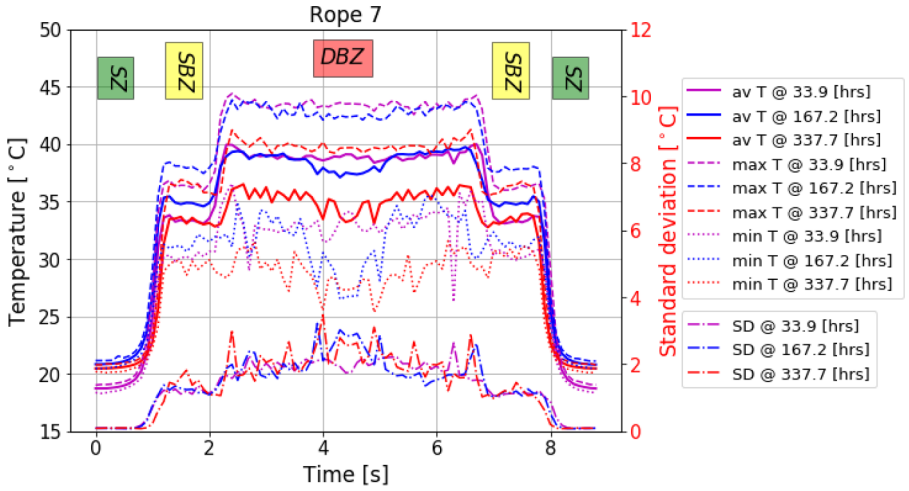

Fig. 16. Rope 7 average, maximum, minimum and standard deviation temperature measurements along the rope for one cycle with respect to the associated test time.

The temperatures are recorded from the portion of the rope visible in the defined ROI, therefore if noticeable twist is present, the displacement of the rope will result in slight differences in temperature recording.

Similar rope degradation and structural rearrangement will result in greater movement of the rope as the test progresses. The ROI is stationary and is chosen so that a portion of the rope will always be visible in the defined boundary. There is greater vertical movement in the rope towards the end of testing instead of the ”smoother” transition of the rope portion visible in the ROI at the start of the test. It is possible this movement can give variation in the measurements.

Noticeable variations in temperature measurement were observed at the transfer points between the SZ to SBZ and SBZ to DBZ sections. The measurement ROI will contain portions from two different bending zones at the transition points and therefore a greater variation of temperatures. Additionally, the largest overall variations are observed at the latter stages of testing in the DBZ sections.

5.3.3. *Application to condition monitoring*

Thermal monitoring using an IR camera brings not only temperature measurements but can provide another useful visual aid to assess the rope surface. The method applied allows each specific bending zone to be scrutinised in detail and monitored over time. Moreover, the results found using the thermal camera in this study allow the physical changes of the rope to be compared concurrently with temperature. Monitoring of the average, maximum, minimum and variation by standard deviation gives information on changes into the physical structure of the rope.

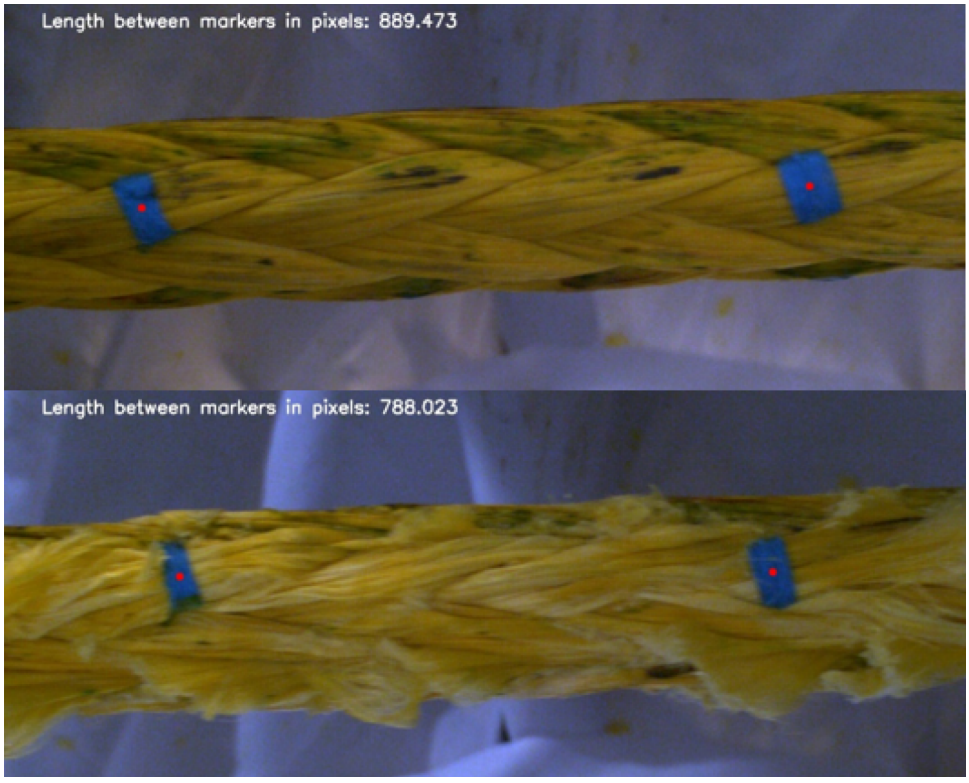

Fig. 17. Subsection DBZ-B-1 in Rope 7 at the beginning of the test (top) and just before rupture (bottom).

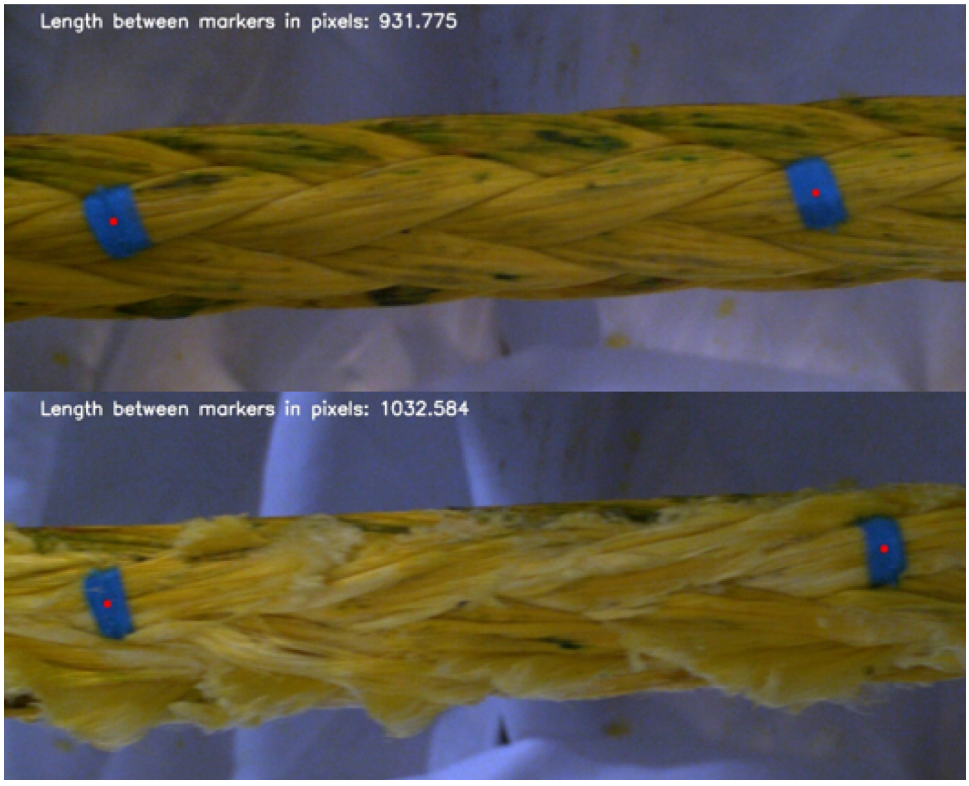

Fig. 18. Subsection DBZ-B-2 in Rope 7 at the beginning of the test (top) and just before rupture (bottom).

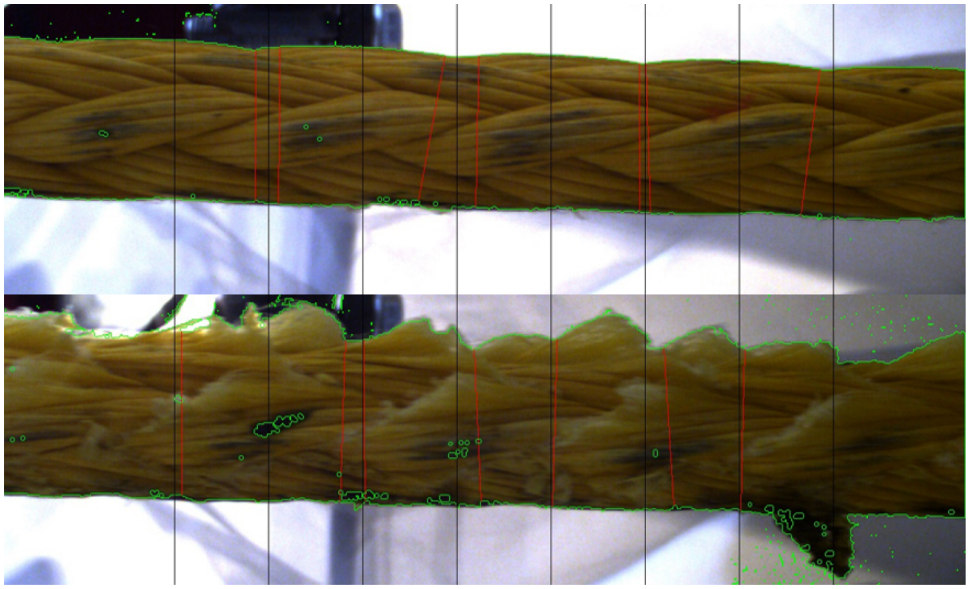

Fig. 19. Section of Rope 3 at the beginning of the test (top) and just before rupture, featuring extruded loops (bottom) as seen from camera 3.

The lower average, maximum and minimum temperatures that coincide with larger standard deviations at more advanced testing stages, particularly in the DBZ section, can be attributed to the increasing presence of structural degradation in the rope. As detected with the width measurement algorithm, the extruded loops and ruptured strands that are visible and more prevalent in the latter stages of testing via the thermal camera, which can be seen in Fig. 20. These degradation features are markedly cooler than the main body of the rope and contribute to the spread of measured temperature values.

The transfer points between the distinct bending zones are also worth investigation. As expected, heat generation will vary due to different bending regimes. The distinct shape indicates that the thermal conductivity in the rope is low and also that the effect of cooling by environment is negligible.

Visible deterioration of the rope will be noticeably more between the SZ and SBZ sections and the SBZ and DBZ sections respectively due to the differences in temperature between the zones. The increasing presence of these cooler temperatures through accumulated damage and effect on temperature measurements serves as an aid to find the exact positions and time for further inspection.

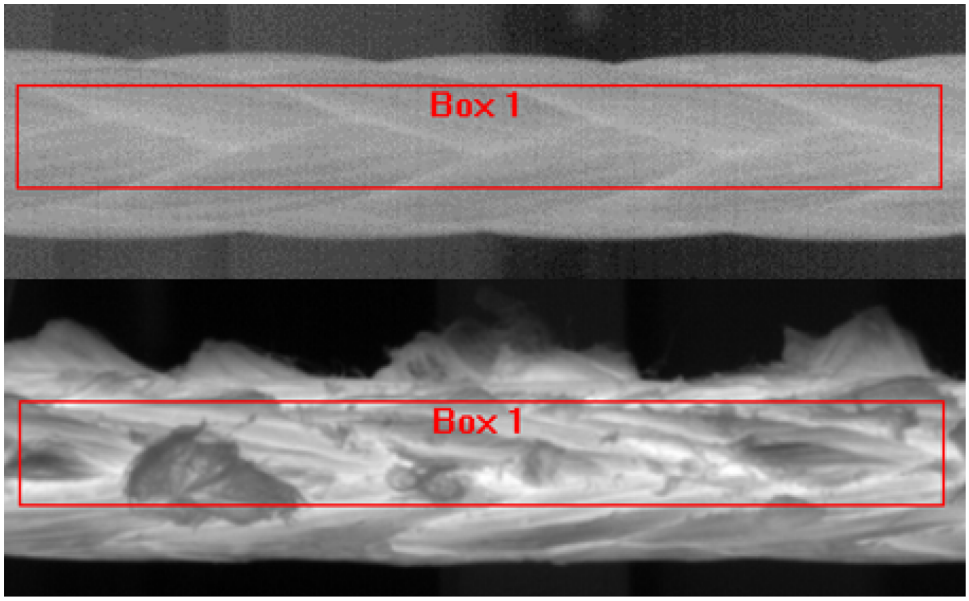

Fig. 20. An example of Rope 7 thermal images at the beginning of the test (top) and just before rupture, featuring extruded loops (bottom) and ruptured strands.

6. Future work

The physical properties of the rope have been measured during repeated deformations in a CBOS regime, thus monitoring the rope state change. For future testing, there is potential for more local length measurements throughout the SBZ and DBZ, with particular emphasis on applying markers to the same sub-rope through the test, rather than just the general area, to gain a better overview of localised changes in the rope condition. Additionally, the tests will make use of higher tensions in order to more accurately reflect safety factors used in industry. Monitoring at these conditions will also give useful insight into how the various condition indicators are influenced in different testing conditions. This will be performed on different types of rope to confirm applicability.

In real application, the same portion of the rope is not subject to constant repeated bending but rather distributed along the rope. This will also involve lifting operations with varying size of payloads instead of a constant applied tension. Additionally there will be differences in moisture and temperature, depending on vessel location and the surrounding environment. These are all factors that have to be considered to for testing and further assess the condition monitoring system effectiveness.

Increased understanding of the underlying physical mechanisms for the changes observed in local length, width and temperature is also required. Changes in the physical structure that occur as damage progresses and its subsequent effect on properties such as thermal conductivity in the rope and heat transfer to the environment require greater understanding. This would mean more informed decision making using the monitoring system and better interpretation of the trends observed in measurement changes.

In the same way inspectors are trained and build up experience by investigating for certain condition indicators during routine visual inspection of rope, there is potential to use machine learning algorithms to detect patterns in rope degradation that cannot be detected by normal visual inspection. The data shows that there are changes in the various measurements that coincide with the deterioration of the rope. These condition indicators can be extended to use as features for machine learning application. A proper understanding of these more subtle changes and identification of deterioration patterns has the potential to develop better RUL estimation for fibre ropes subject to CBOS regimes.

7. Conclusions

This paper presented results from a computer vision monitoring system, thermal camera and distance measuring laser to monitor the deterioration in ropes subjected to a CBOS regime. The computer vision algorithms presented are capable of detecting localised length changes subject to appropriate marking in the rope, as well as detecting rope damage such as extruded loops and ruptured strands through cross width detection. The deterioration of the rope can also be monitored via thermal imaging, as it is capable of detecting temperature changes that coincide with structural deterioration in the latter stages of testing.

This combination of monitoring gives useful insight into fibre rope condition from different perspectives and emphasises the need for localised strand-level monitoring at specific sections in the rope. However, if longitudinal distortion is to be used, then a thorough and consistent account of the rope pattern and structure is needed, given the demonstrated potential for variations.

Ultimately, the detection of changes over time can be used as condition indicators and can be engineered into features in application of machine learning algorithms to classify damage and better gauge RUL for fibre rope subject to CBOS regimes.

CRediT authorship contribution statement

Shaun Falconer: Conceptualization, Methodology, Software, Validation, Formal analysis, Investigation, Data curation, Writing - original draft, Writing - review & editing, Visualization. **Ellen Nordgård-Hansen:** Methodology, Data curation, Resources, Writing - review & editing, Supervision, Project administration. **Geir Grasmo:** Conceptualization, Resources, Methodology, Writing - review & editing, Supervision.

Declaration of Competing Interest

The authors declare that they have no known competing financial interests or personal relationships that could have appeared to influence the work reported in this paper.

Acknowledgments

The research presented in this paper has received funding from the

Norwegian Research Council, SFI Center for Offshore Mechatronics, project number 237896. The authors would also like to extend an extra special thanks to Benyamin Akdemir for his assistance in creating the experiment set up and his insight into the use of machine vision cameras and also to Yannick Bafanga for automating the task of retrieving the thermal image statistics.

Appendix A. Instrumentation details

Table 3
Optical camera specification.

Property	Value
Maximum frame rate	169 fps
Resolution	1.3 MP
Pixels (H x V)	1280 x 1024
Pixel size	4.8 x 4.8 μm

Table 4
Thermal camera specification.

Property	Value
Image acquisition	0.0015 Hz to 125 Hz
Temperature range	-20 °C to 350 °C
Pixels (H x V)	640 x 512
Accuracy	± 2 °C or ± 2% of reading

Table 5
Distance measuring laser specification.

Property	Value
Typical measuring tolerance	+/- 2.0 mm
Typical range	40 m

References

[1] DNVGL, DNVGL-RP-E304: Damage Assessment of Fibre Ropes for Offshore Mooring, (2017). July 2017.
[2] CI 2001-04: Fiber Rope Inspection and Retirement Criteria, (2004).
[3] DNVGL, DNVGL-OS-E303: Offshore fibre ropes, (2018). July 2018.
[4] DNVGL, DNVGL-ST-E407: Rope Based Deployment and Recovery Systems for Designated Service, (2016).
[5] DNVGL, DNVGL-RP-E305: Design, testing and analysis of offshore fibre ropes, (2015). September 2015.
[6] P. Davies, M. François, N. Lacotte, T.D. Vu, D. Durville, An empirical model to predict the lifetime of braided HMPE handling ropes under cyclic bend over sheave (CBOS) loading, Ocean Eng. 97 (2015) 74–81, https://doi.org/10.1016/j.oceaneng.2015.01.003.
[7] J. Hearle, I. Overington, M.S. Overington, Non-contact strain and deformation measurement in yarns, ropes and fabrics, IFAI Expo, (2001).
[8] S.R. Ghoreishi, P. Davies, P. Cartraud, T. Messager, Analytical modeling of synthetic fiber ropes. part II: a linear elastic model for 1 + 6 fibrous structures, Int. J. Solids Struct. 44 (9) (2007) 2943–2960, https://doi.org/10.1016/j.ijsolstr.2006.08.032.
[9] R. Söhnchen, Securing safety of ropes with a visual rope inspection system, OIPEEC Conference Proceedings 2015, (2015). March.
[10] O. Yaman, M. Karakose, Auto correlation based elevator rope monitoring and fault detection approach with image processing, IDAP 2017 - International Artificial Intelligence and Data Processing Symposium, (2017), https://doi.org/10.1109/IDAP.2017.8090176.
[11] I. Mupende, H. Zerza, US 2014/0027401 A1: APPARATUS FOR RECOGNIZING THE DISCARD STATE OF A HIGH-STRENGTH FIBER ROPE IN USE IN LIFTING GEAR, 2014, 10.1016/j.micromeso.2003.09.025.
[12] F.B. van der Woude, J.A. Zijlmans, US 2017/0045493 A1: REAL-TIME ROPE MONITORING, 2017.
[13] B. Ernst, E. Rührnössl, R. Kirth, P. Baldinger, R. Traxl, G. Kaiser, US 2018/0363241 A1: METHOD FOR DETERMINING THE REPLACEMENT STATE OF WEAR OF A ROPE MADE OF A TEXTILE FIBRE MATERIAL, 2018.
[14] C. De Angelis, US6247359 B1: Aparatus for identification of need to replace synthetic fiber ROPES,1999,10.1126/science.Liquids.
[15] D.E. Logan, L.H. Favrow, R.J. Haas, P.A. Stucky, N.R. Baldwin, US 7117981B2: load bearing member for use in an elevator system having external markings for indicating a condition of the assembly, 2006.
[16] R. Törnqvist, M. Strande, D. Cannell, P. Gledhill, P. Smeets, D.S.M. Dyneema, Deployment of Subsea Equipment : Qualification of Large Diameter Fibre Rope for Deepwater Construction Applications, Offshore Technology Conference, (2011).
[17] P. Davies, N. Lacotte, G. Kibsgaard, R. Craig, D. Cannell, S. Francois, O. Lodeho, K. Konate, S. Mills, M. François, A.-L. Defoy, D. Durville, D. Vu, J. Gilmore, D. Sherman, Bend Over Sheave Durability of Fibre Ropes for Deep Sea Handling Operations, Proceedings of the ASME 2013 32nd International conference on Ocean, Offshore and Arctic Engineering, (2013), pp. 1–8.
[18] E. Nordgård-Hansen, H.J. Hassel, R. Schlanbusch, Chemometrics as a tool to gain insight into fiber rope aging from infrared images, Proc. Annual Conf. PHM Soc. 11 (1) (2019) 1–13, https://doi.org/10.36001/phmconf.2019.v11i1.598.
[19] A. De Angelis, US6392551: SYNTHETIC FIBER CABLE WITH TEMPERATURE SENSOR, 2 (12) (2002).
[20] F. Ning, X. Li, N.O. Hear, R. Zhou, Thermal failure mechanism of fiber ropes when bent over sheaves, Text. Res. J. (2018), https://doi.org/10.1177/0040517518767147.
[21] S. Falconer, A. Gromsrud, E. Oland, G. Grasmo, Preliminary Results on Condition Monitoring of Fiber Ropes using Automatic Width and Discrete Length Measurements, Annual Conference of the Prognostics and Health Managemet Society 2017, (2017).
[22] G. Bradski, The opencv library, Dr. Dobb's J. Softw. Tools (2000).